Abstract

Quantum Chromo-Dynamics (QCD) is the theory describing the strong interactions between quarks and gluons, the fundamental constituents of hadrons. Lattice QCD calculations predict a transition from colour-neutral hadrons to a colour-deconfined state called Quark-Gluon Plasma (QGP) under extreme temperature and energy density conditions, which can be reached in the laboratory by colliding high-energy heavy ions.

Heavy-flavour quarks (charm and beauty) are produced in the earliest stages of the collision and interact with the formed medium, losing energy through interactions with its constituents, making heavy-flavour hadrons excellent probes of the properties of the QGP. The hadronisation process is the transition from colour-charged partons (quarks and gluons) produced in a collision into colour-neutral hadrons. Predictions assuming its universality (i.e., independence from the collision system and energy) typically parametrise this process from results obtained in e^+e^- collisions but fail in describing the measured charm-baryon production measured in proton-proton (pp) and p–Pb collisions at the Large Hadron Collider (LHC), suggesting that the hadronisation process is not universal. The hadronisation mechanism is expected to be modified by the presence of the QGP, as a novel process, called recombination, is expected to occur. In this process, the produced heavy-flavour quarks combine with other quarks from the medium to form hadrons. The observed baryon enhancement in pp collisions is qualitatively described by models that include QGP droplets formation, as well as by event generators such as Pythia 8 in which colour reconnections are considered in modelling the parton shower and the fragmentation in the parton-rich environment created in pp collisions at the LHC.

In the presence of QGP, the production of strange quarks is expected to be enhanced due to the increase in their thermal production owing to the high temperatures reached. An increased production of strange hadrons relative to pions is observed in Pb–Pb collisions with respect to pp collisions, where the production of QGP is not expected. However, a smooth increase of strange-hadron relative abundances with the number of charged-particles produced in the collision has been observed in pp collisions, raising the question of whether small droplets of QGP could also be produced in high-multiplicity pp collisions.

Therefore, because of the recombination mechanism and the enhanced production of strange quarks, an increase in the strange over non-strange $\mathrm{D_s^+/D^+}$ production yield ratio is expected in the presence of QGP.

The ALICE detector installed at the LHC is designed to address the physics of strongly-interacting matter and QGP produced in ultra-relativistic heavy-ion collisions. During the LHC Long Shutdown 2 (2019–2021) the detector was upgraded by enhancing the tracking performance and increasing the readout rate to collect larger data samples, improving its capabilities to probe the QGP with heavy-flavours.

This Thesis is devoted to the precise measurement of the transverse-momentum-(p_{T}-)differential $\mathrm{D_s^+/D^+}$ production-yield ratio at midrapidity ($|y| < 0.5$) in pp collisions at $\sqrt{s} = 13.6$ TeV with the data collected by the ALICE experiment during

the ongoing LHC Run 3 data-taking period. This ratio of strange over non-strange charm meson yields allows for a direct access to information on charm-quark hadronisation mechanisms. Due to their small lifetime ($\tau \sim 100 - 300$ µm/c), $\mathrm{D_s^+}$ and $\mathrm{D^+}$ mesons cannot be directly detected and are reconstructed through their decay products. They are reconstructed through the same hadronic decay channel

$$\mathrm{D_s^+, D^+} \rightarrow \phi\pi^+ \rightarrow \mathrm{K^+K^-}\pi^+ \quad ,$$

allowing for the cancellation of some of the systematic uncertainties related to the measurement. Multiclass Machine Learning (ML) algorithms have been employed to suppress the large combinatorial background arising from the combination of three independent tracks produced in the pp collision and increase the statistical significance of the measurement. Additionally, the ML-based selections were used to increase the relative contribution of prompt $\mathrm{D_s^+}$ and $\mathrm{D^+}$ mesons (i.e., those directly produced in the hadronisation of a charm quark or through the strong decay of a directly produced excited charm hadron or charmonium state) in the selected sample. The signal is extracted in 14 p_{T} intervals within the $0.5 < p_{\mathrm{T}} < 24$ GeV/c range by fitting the invariant mass distribution of candidates passing the ML selections.

The extracted signal is then corrected for the geometrical acceptance of the ALICE detector, the selection efficiency, and the residual non-prompt contamination arising from D mesons produced in the decay of a beauty hadron and surviving the ML selections. The corrections are obtained from Monte Carlo simulations.

The measured $\mathrm{D_s^+/D^+}$ production-yield ratio is compared to results obtained by the ALICE Collaboration with the data collected during the LHC Run 2 data-taking period at the different centre-of-mass energies of $\sqrt{s} = 5.02, 7$, and 13 TeV and with measurements performed by the LHCb Collaboration at the LHC in the forward-rapidity range $2.0 < y < 4.5$ in pp collisions at $\sqrt{s} = 13$ TeV. The results are compatible with those obtained in Run 2 by both ALICE and LHCb Collaborations, indicating no significant dependence of the $\mathrm{D_s^+/D^+}$ ratio on the centre-of-mass energy and rapidity. Thanks to the larger data samples collected during the LHC Run 3 data-taking period, a more precise and granular measurement of the $\mathrm{D_s^+/D^+}$ production-yield ratio than that measured in Run 2 is achieved. Furthermore, the p_{T} reach of the measurement has been extended to lower values, reaching as low as 0.5 GeV/c. These measurements provide state-of-the-art results on the production of charm-strange mesons in pp collisions.

Lastly, to study the performance of the ALICE experiment in heavy-ion collisions, the reconstruction of $\mathrm{D_s^+}$ and $\mathrm{D^+}$ mesons was performed in Pb–Pb collisions at $\sqrt{s_{\mathrm{NN}}} = 5.36$ TeV for different centrality intervals, which represent the degree of overlap of the two colliding nuclei, using rectangular selection criteria. The results in the 10–30% centrality class have been used as benchmarks of the performance of the upgraded ALICE experiment in heavy-ion collisions. These results will provide a solid baseline for the study of the $\mathrm{D_s^+/D^+}$ production-yield ratio in Pb–Pb collisions, to be performed in the future. By comparing the results obtained in Pb–Pb collisions and the measurements in pp collisions described in this Thesis, insights into the hadronisation mechanisms of charm quarks in the presence of the QGP, where strange quarks are more abundant, will be obtained.

Chapter 8

$\mathrm{D_s^+}$ and $\mathrm{D^+}$ mesons reconstruction in Pb–Pb collisions

The work presented in this Thesis so far has focused on the study of the $\mathrm{D_s^+/D^+}$ production-yield ratio in pp collisions at $\sqrt{s} = 13.6$ TeV, which can provide information on the hadronisation of charm quarks. This serves also as a baseline for studies in pp collisions as a function of charged-particle multiplicity, to search for the effects of a possible production of small QGP droplets in small collision systems. Moreover, it also provides a precise reference for measurements in heavy-ion collisions, where an extended deconfined phase is expected to be formed. Measurements of $\mathrm{D_s^+}$-meson production in Pb–Pb collisions have been performed by the ALICE Collaboration at the centre-of-mass energies per nucleon-nucleon collision of $\sqrt{s_{\mathrm{NN}}} = 5.02$ TeV [1, 2] and $\sqrt{s_{\mathrm{NN}}} = 2.76$ TeV [3]. The measured R_{AA} of prompt $\mathrm{D_s^+}$ mesons in central and semicentral Pb–Pb collisions is compatible within uncertainties with that of other non-strange D mesons ($\mathrm{D^0}, \mathrm{D^+}$, and $\mathrm{D^{*+}}$) for $p_{\mathrm{T}} \gtrsim 10$ GeV/c, where the hadronisation process is expected to occur mainly via fragmentation. At lower p_{T}, where the coalescence mechanism is expected to play a more relevant role, the measured R_{AA} of prompt $\mathrm{D_s^+}$ mesons is systematically higher than that of non-strange D mesons, although the results are compatible within one standard deviation. In addition, while the measured production-yield ratio of non-strange over non-strange D mesons ($\mathrm{D^+/D^0}$ and $\mathrm{D^{*+}/D^0}$) is found to be compatible in Pb–Pb and pp collisions, indicating no significant modification of their relative abundances as a function of p_{T} and centrality, the production-yield ratio of strange over non-strange D mesons ($\mathrm{D_s^+/D^+}$ and $\mathrm{D_s^+/D^0}$) is found to be larger in central (semicentral) Pb–Pb collisions than in pp collisions, but the measurements in the two systems are compatible within about 2.3 (2.4) standard deviations. The large uncertainties of the measurements in Pb–Pb collisions available so far did not allow for drawing firm conclusions on the production mechanism of $\mathrm{D_s^+}$ mesons in heavy-ion collisions. Additionally, the measurement is performed for $p_{\mathrm{T}} > 2$ GeV/c. About 70% of the produced D mesons have p_{T} below this threshold [4], and therefore the results cannot disentangle a possible modification of the p_{T} spectrum from an enhancement of the $\mathrm{D_s^+}$ meson production in Pb–Pb collisions with respect to pp collisions.

Thanks to the upgrade of the ALICE detector during the LHC Long Shutdown 2, the experiment significantly enhanced its readout rate in Pb–Pb collisions to more

than 50 times that achieved during the LHC Run 2 data-taking period, and improved its spatial resolution by a factor of about 2, allowing for a better separation of displaced decay vertices [5]. These upgrades will allow for enhancing the precision of the measurements of rare probes, such as heavy-flavour hadrons, and for completely new insights into the properties of the QGP, such as the exclusive reconstruction of beauty-hadron decays. With the improvements in the detector capabilities, the strange over non-strange D-meson production-yield ratios can be measured with unprecedented precision in Pb–Pb collisions, providing more significant evidence, or the lack thereof, of the enhancement of D_s^+-meson production in the hadronisation of the QGP, due to the enhancement of stange-antistrange quark pairs and the hadronisation of charm quarks via recombination.

At the time of starting the work presented in this Thesis, the ALICE Collaboration was performing the first collisions of ultra-relativistic lead ions with the upgraded apparatus. Therefore, rapid feedback on the quality of the data was required. Since the upgrade of the ALICE detector mainly focused on the improvement of its capabilities for heavy-flavour measurements, particular attention was given to the performance of the reconstruction of D mesons. Hence, the first studies carried out for this Thesis were devoted to the reconstruction of D mesons in Pb–Pb collisions. In this Chapter, the analysis strategy and the results of the reconstruction of D_s^+ and D^+ mesons in Pb–Pb collisions at $\sqrt{s_{\rm NN}} = 5.36$ TeV are presented.

8.1 Event selection and data sample

The analysis reported in this Chapter is performed on a dataset of Pb–Pb collisions at a centre-of-mass energy per nucleon pair of $\sqrt{s_{\rm NN}} = 5.36$ TeV, collected by the ALICE Collaboration during the 2023 data-taking period. Since the calibration of the tracking detectors was still ongoing at the time of the analysis, and because the reconstruction of Pb–Pb events is very resource-intensive, only a fraction of 20% of the total data sample collected during the 2023 data-taking period was made available and therefore analysed. Only once the quality of the reconstruction of Pb–Pb events was validated, the full dataset was processed.

The data sample is collected using a Minimum-Bias trigger (the `Sel8` trigger), which selects events that satisfy the requirement of having a signal coincidence in the FT0-A and FT0-C detectors. The centrality of the collision is determined using the signal amplitude of the forward-rapidity FT0-C detector, which is proportional to the number of particles produced in the pseudorapidity interval $-3.3 < \eta < -2.1$. The centrality classes are defined as percentiles of the inelastic cross-section and are determined starting from the charged-particle multiplicity distribution obtained with the FT0-C detector (which is calibrated for each data-taking period). Collisions in the 0–10% centrality class are the most central, with the largest number of produced charged particles.

The analysed centrality classes are the 10–30%, 30–50%, and 60–90%, but no signal was visible in the last centrality class on the small data sample used for these checks.

8.2 $\mathrm{D_s^+}$ and $\mathrm{D^+}$ mesons reconstruction

$\mathrm{D_s^+}$ and $\mathrm{D^+}$ mesons are reconstructed in the same decay channel exploited for the measurement of the $\mathrm{D_s^+/D^+}$ production-yield ratio in pp collisions presented in the previous Chapters:

$$\mathrm{D_s^+, D^+ \to \phi\pi^+ \to K^+K^-\pi^+} \quad .$$

In the most central Pb–Pb collisions, around 21500 charged particles are produced on average [6]. Therefore, the reconstruction of D mesons in ultra-relativistic heavy-ion collisions is more challenging than in pp collisions since a much larger combinatorial background from the combination of three uncorrelated tracks is produced. On the other hand, the higher number of tracks in Pb–Pb collisions allows for a more precise reconstruction of the primary vertex position. Thereby, a slight improvement in the separation of the signal from the background, by exploiting the displaced decay topology of the D mesons, is achieved as compared to pp collisions.

Furthermore, with the replacement of the TPC MultiWire Proportional Chambers readout chambers with Gas Electron Multipliers performed during the LHC Long Shutdown 2 upgrade, the amount of backflow of ions in the TPC has significantly increased as compared to the LHC Run 2 data-taking period. The residual ions in the TPC gas volume can distort the electric field, leading to a distortion of the drift paths of the electrons produced by the ionising particles that are intended to be detected. This effect is particularly relevant in the track reconstruction, as it worsens the spatial and momentum resolution and the track reconstruction efficiency. Despite a great effort in the calibration of the TPC, the backflow of ions is still not fully corrected for, and affects the track reconstruction performance. This leads to a worse quality in the reconstruction of $\mathrm{D_s^+}$ and $\mathrm{D^+}$ mesons, as the broadening of their signal peaks, due to the non-optimal momentum resolution causes a worsening of the signal to background ratio and may lead to an overlap of their invariant mass distributions given the small mass difference of about 10 MeV/c^2.

Lastly, at the time this work was carried out, Monte Carlo simulations of Pb–Pb collisions enriched with heavy-flavour hadrons were not available. Therefore, there was no possibility of employing Machine Learning (ML) techniques to select the D-meson candidates, as it is done for the analysis of the $\mathrm{D_s^+/D^+}$ production yield ratio in pp collisions described in the previous Chapters, since a pure data sample of signal candidates needed to train the ML model was not available.

Therefore, the selection of D-meson candidates is performed using rectangular selection criteria exploiting the displaced decay topology of heavy-flavour hadrons and their decay kinematics. Additionally, particle identification techniques of the decay products are employed to reduce the combinatorial background and select $\mathrm{D_s^+}$ and $\mathrm{D^+}$ candidates. Selections based on the same variables used in the pp analysis, such as the decay length, pointing angle, and kinematical variables based on the production of a ϕ meson in the considered decay channel of the $\mathrm{D_s^+}$ and $\mathrm{D^+}$ mesons ($|\Delta M(\mathrm{KK})|$, $\cos(\theta'(\mathrm{K}))$) described in Chapter **??** are applied. Since the number of particles produced in a heavy-ion collision varies drastically with the centrality of the collision, the selection criteria employed for the selection of D-meson signals were optimised independently for each centrality class.

For each centrality interval, the selection criteria are optimised by testing different sets of cut values and maximising the statistical significance of the extracted $\mathrm{D_s^+}$-meson signal, for each considered p_T interval. This strategy is used as no physics observables are meant to be extracted from the analysis, and the main goal is to validate the reconstruction framework and provide feedback on its performance. In fact, the maximisation of the statistical significance of the signal on the same sample used for the yield extraction should not be pursued as a strategy for the selection of D-meson candidates in physics analyses, as statistical fluctuations can lead to a bias in the extracted yields.

Table 8.1: Variation range and number of steps for the variables used in the optimisation of the selection criteria for the selection of $\mathrm{D_s^+}$- and $\mathrm{D^+}$-meson candidates in Pb–Pb collisions at $\sqrt{s_\mathrm{NN}} = 5.36$ TeV.

			p_T (GeV/c)				
Variable	N. steps		2–4	4–6	6–8	8–12	12–24
$L(\mu\mathrm{m}) >$	3	min	200	200	200	200	200
		max	600	800	800	800	800
$\cos\theta_\mathrm{p} >$	4	min	0.9900	0.9980	0.9980	0.9800	0.9800
		max	0.9990	0.9995	0.9995	0.9950	0.9950
$\cos\theta_\mathrm{p}^{xy} >$	4	min	0.9900	0.9970	0.9980	0.9800	0.9800
		max	0.9990	0.9985	0.9995	0.9950	0.9950
$\lvert\Delta M(\mathrm{KK})\rvert(\mathrm{MeV}/c^2) <$	3	min	5	5	5	5	5
		max	9	9	9	9	9
$\lvert\cos^3(\theta'(\mathrm{K}))\rvert >$	3	min	0.1	0.1	0.1	0.1	0.1
		max	0.3	0.3	0.3	0.3	0.3
$\chi^2_\mathrm{PCA} <$	4	min	3	3	3	3	3
		max	12	12	12	12	12

The configuration used for the optimisation of the set of selection criteria employed for the selection of $\mathrm{D_s^+}$ and $\mathrm{D^+}$ meson candidates is reported in Table 8.1, where the variables used, the considered variation range, and the number of intermediate steps are reported. A total of 1728 selection criteria were considered for each p_T interval of the different centrality classes. In addition to those reported in Table 8.1, a few additional variables are used to further improve the selection of $\mathrm{D_s^+}$ and $\mathrm{D^+}$ mesons, but their thresholds are not optimised. The normalised decay length in the transverse plane is required to be larger than 2, and the PID information on the three daughter tracks from both the TPC and TOF detectors is exploited by requiring that the $|\mathrm{n}\sigma|$ with respect to the pion (kaon) expected signal is at most equal to 4. As for the analysis performed in pp collisions, the information from the TOF detector was used when available, but not required.

Figure 8.1 illustrates the results for the optimisation of the $\mathrm{D_s^+}$ meson statistical significance in the 10–30% centrality class for the 2–4 GeV/c p_T interval, by reporting the statistical significance as a function of the set of applied selections identified by an index. The large steps in the statistical significance dividing the graph into three parts are due to the different thresholds applied to the candidate decay length.

Smaller periodic modulations of the D_s^+ statistical significance are also observed and are due to the different thresholds applied to the other considered variables.

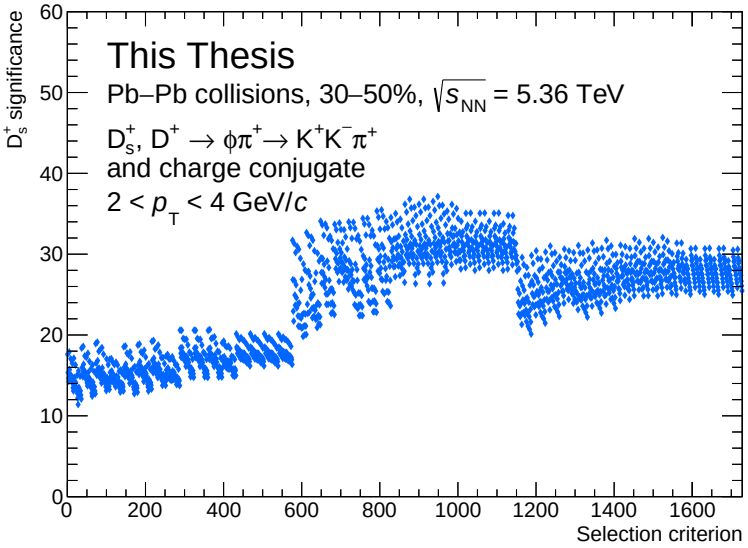

Figure 8.1: D_s^+-meson signal statistical significance as a function of the selection criteria for the $2 < p_T < 4$ GeV/c interval in the 30–50% centrality class.

The optimal selection criteria for the selection of D_s^+ meson candidates in the 10–30% and 30–50% centrality classes are reported in the Tables 8.2 and 8.3, respectively. The optimal selection criteria for the 60–90% centrality class are not reported, as no signal was extracted in this centrality class.

Table 8.2: Optimal selection criteria for the selection of D_s^+ meson candidates in the 10–30% centrality class.

	p_T interval (GeV/c)				
Variable	2−4	4−6	6−8	8−12	12−24
$L(\mu m) >$	600	200	500	200	200
$\cos\theta_p >$	0.9900	0.9980	0.9985	0.9800	0.9800
$\cos\theta_p^{xy} >$	0.9990	0.9980	0.9980	0.9900	0.9950
$\lvert\Delta M(KK)\rvert(MeV/c^2) <$	7	9	5	7	7
$\lvert\cos^3(\theta'(K))\rvert >$	0.3	0.2	0.2	0.2	0.3
$\chi^2_{PCA} <$	3.0	6.0	3.0	3.0	9.0

8.3 Signal extraction

Once the selection criteria are optimised for each p_T interval and centrality class, the signal is extracted by fitting the invariant mass distribution of the selected candidates. The fit function is composed of an exponential function for describing the

Table 8.3: Optimal selection criteria for the selection of D_s^+ meson candidates in the 30–50% centrality class.

	p_T interval (GeV/c)				
Variable	2−4	4−6	6−8	8−12	12−24
$L(\mu m) >$	400	200	200	200	200
$\cos\theta_p >$	0.996	0.998	0.998	0.980	0.995
$\cos\theta_p^{xy} >$	0.996	0.997	0.998	0.985	0.980
$\lvert\Delta M(KK)\rvert(MeV/c^2) <$	7	9	9	5	5
$\lvert\cos^3(\theta'(K))\rvert >$	0.1	0.1	0.1	0.1	0.2
$\chi^2_{PCA} <$	3.0	3.0	12.0	12.0	9.0

background shape and two Gaussian functions for the D_s^+ and D^+ signal peaks. The correlated background from $D^+ \to \pi^+K^-\pi^+$ introduced in Chapter **??** is not included, as the absence of MC simulations precludes the estimation of its shape. The fit of the invariant mass distributions of the candidates passing the selection criteria described above is performed in the invariant mass range of $1.7 < M < 2.1$ GeV/c^2. A clear signal peak is observed in both the 10–30% and 30–50% centrality classes, with statistical significances ranging from 14 to 35 for D_s^+ mesons and from 4 to 14 for D^+ mesons depending on p_T in the 10–30% centrality interval, and from 9 to 37 for D_s^+ mesons and from 4 to 21 for D^+ mesons in the 30–50% centrality class. Figure 8.2 shows the normalised invariant mass distribution of D-meson candidates passing the applied selections in the $2 < p_T < 4$ GeV/c (top-left panel) and $6 < p_T < 8$ GeV/c (bottom-left panel) intervals of the 10–30% centrality class and in the $4 < p_T < 6$ GeV/c (top-right panel) and $8 < p_T < 12$ GeV/c (bottom-right panel) intervals of the 30–50% centrality class.

As mentioned above, one of the consequences of the backflow of ions in the TPC is the distortion of the drift paths of the ionised electrons, which leads to a worsening of the track momentum resolution. An increase of the peak widths with increasing p_T is already visible in Fig. 8.2: while the D_s^+ and D^+ peaks are well separated in both the $2 < p_T < 4$ GeV/c and $4 < p_T < 6$ GeV/c intervals, at the higher p_T intervals of $6 < p_T < 8$ GeV/c and $8 < p_T < 12$ GeV/c the peak widths are larger, and the two peaks are partially overlapping. Nevertheless, a worsening in the resolution with increasing p_T is expected due to the reduced track curvature in the presence of the magnetic field. Therefore, to test the validity of the distortion corrections in the reconstruction framework it is useful to study the resolution of the D_s^+ and D^+ mesons peaks, and compare it with that obtained during the LHC Run 2 data-taking period, where fewer distortions were present thanks to the reduced interaction rate and the active ion gates. Similar studies are being performed for the $K_s^0 \to \pi^+\pi^-$ peaks. However, the measurement of D meson widths allows the test of a different p_T range of the tracks and the effects on the charged kaon reconstruction, which is not possible with the K_s^0 mesons.

The resolution of the D_s^+ and D^+ mesons peaks is extracted from the fits of the invariant mass distribution of the selected candidates as the standard deviation of the Gaussian function used to describe the D-meson signals. In Figure 8.3, the peak

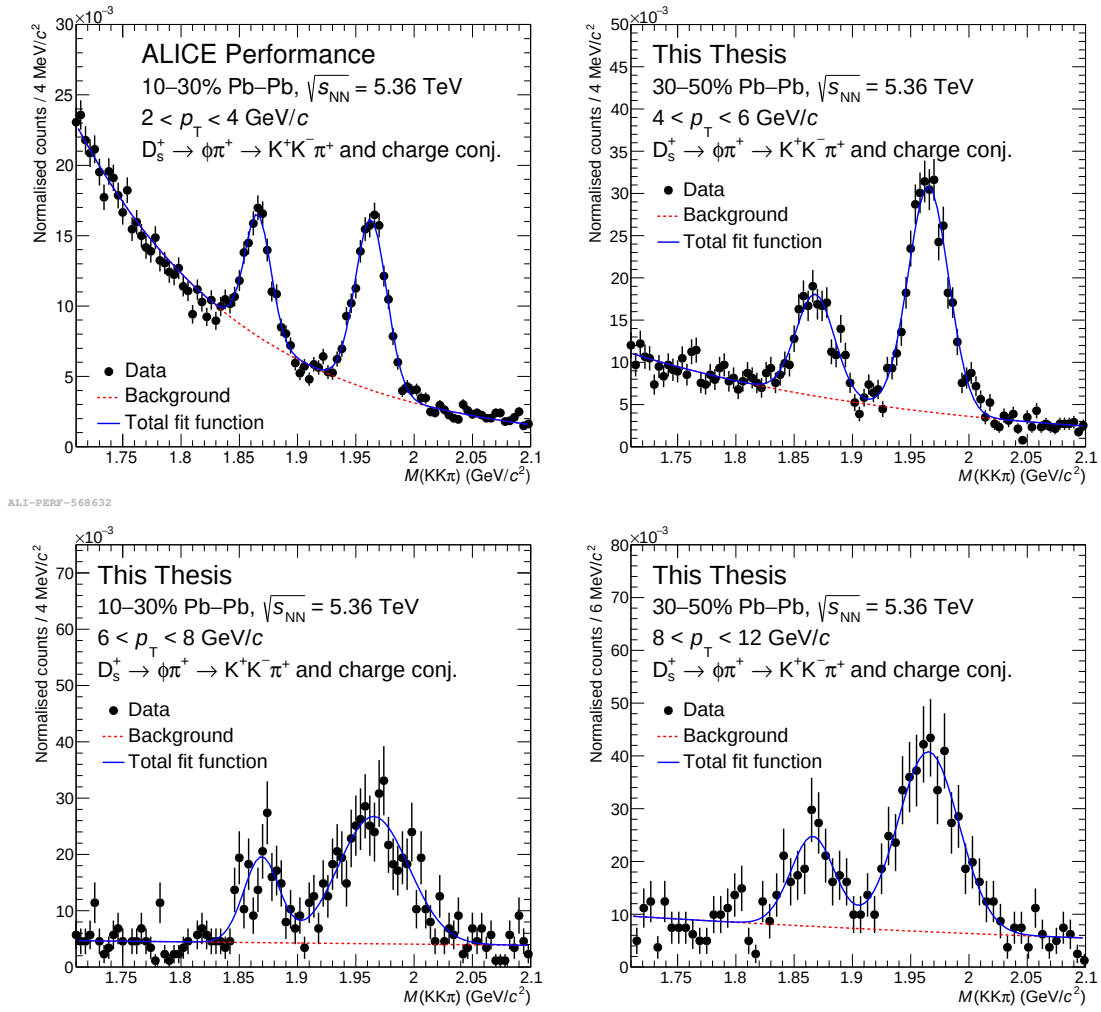

Figure 8.2: Normalised invariant mass distribution of the selected D-meson candidates in the $2 < p_{\mathrm{T}} < 4$ GeV/c (top-left panel) and $6 < p_{\mathrm{T}} < 8$ GeV/c (bottom-left panel) intervals of the 10–30% centrality class and in the $4 < p_{\mathrm{T}} < 6$ GeV/c (top-right panel) and $8 < p_{\mathrm{T}} < 12$ GeV/c (bottom-right panel) intervals of the 30–50% centrality class.

width of the D_s^+ meson signal is shown for the analysis performed in this Thesis using the 30–50% centrality class of Pb–Pb collisions recorded in the LHC Run 3 data-taking period (blue markers) as a function of p_T. A clear increasing trend of the peak width with p_T is observed, and is attributed to the worsening of the momentum resolution with increasing p_T due to the smaller curvature of high-momentum tracks. The peak widths of the D_s^+-meson signals extracted from the Pb–Pb collisions data collected during the LHC Run 2 data-taking period at $\sqrt{s_{NN}} = 5.02$ TeV in the 30–50% centrality class [1] (shown as green markers in Fig. 8.3) are smaller than those found for Run 3 samples. This is due to the distortions of the electric field in the TPC, which were smaller in Run 2 because the TPC ion backflow was significantly suppressed using active gating grids. Lastly, the peak widths of the D_s^+-meson signals extracted from pp collisions data recorded during the LHC Run 3 data-taking period at $\sqrt{s} = 13.6$ TeV in this Thesis (as described in Chapter **??**) are reported as a function of p_T with red markers. These results show a magnitude of the width and a trend with p_T which are consistent with what is observed in Pb–Pb collisions at $\sqrt{s_{NN}} = 5.36$ TeV, confirming that the observed worsening of the momentum resolution is due to the backflow of ions in the TPC, which affect similarly the different samples of pp and Pb–Pb collisions collected during the LHC Run 3 data-taking period. The widths extracted in pp collisions are systematically smaller than those from Pb–Pb collisions, albeit being compatible within uncertainties. This effect may be due to a newer reconstruction performed in the pp collisions data, which may have improved the momentum resolution. Studies are currently ongoing to further improve the calibration of the reconstruction and improve the momentum resolution in both pp and Pb–Pb collisions, allowing for more precise measurements of the production of D mesons.

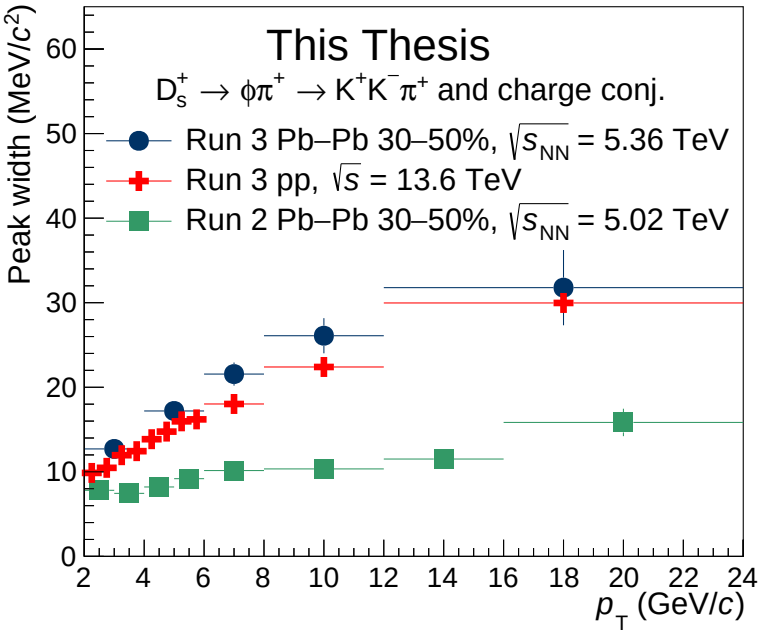

Figure 8.3: Width of the D_s^+-meson signal peak as a function of p_T measured in Pb–Pb collisions at $\sqrt{s_{NN}} = 5.36$ TeV in the 30–50% centrality class and pp collisions at $\sqrt{s} = 13.6$ TeV recorded during the LHC Run 3 data-taking period (blue and red markers, respectively) and in the 30–50% centrality class of Pb–Pb collisions at $\sqrt{s_{NN}} = 5.02$ TeV recorded during the LHC Run 2 data-taking period (green markers).

Bibliography

[1] **ALICE** Collaboration, S. Acharya *et al.*, "Measurement of prompt $\mathrm{D_s^+}$-meson production and azimuthal anisotropy in Pb–Pb collisions at $\sqrt{s_{\mathrm{NN}}} = 5.02$ TeV", *Phys. Lett. B* **827** (2022) 136986, arXiv:2110.10006 [nucl-ex].

[2] **ALICE** Collaboration, S. Acharya *et al.*, "Measurement of $\mathrm{D^0}$, $\mathrm{D^+}$, $\mathrm{D^{*+}}$ and $\mathrm{D_s^+}$ production in Pb-Pb collisions at $\sqrt{s_{\mathrm{NN}}} = 5.02$ TeV", *JHEP* **10** (2018) 174, arXiv:1804.09083 [nucl-ex].

[3] **ALICE** Collaboration, J. Adam *et al.*, "Measurement of $\mathrm{D_s^+}$ production and nuclear modification factor in Pb-Pb collisions at $\sqrt{s_{\mathrm{NN}}} = 2.76$ TeV", *JHEP* **03** (2016) 082, arXiv:1509.07287 [nucl-ex].

[4] **ALICE** Collaboration, S. Acharya *et al.*, "Prompt $\mathrm{D^0}$, $\mathrm{D^+}$, and $\mathrm{D^{*+}}$ production in Pb–Pb collisions at $\sqrt{s_{\mathrm{NN}}} = 5.02$ TeV", *JHEP* **01** (2022) 174, arXiv:2110.09420 [nucl-ex].

[5] **ALICE** Collaboration, "ALICE upgrades during the LHC Long Shutdown 2", arXiv:2302.01238 [physics.ins-det].

[6] **ALICE** Collaboration, J. Adam *et al.*, "Centrality dependence of the pseudorapidity density distribution for charged particles in Pb-Pb collisions at $\sqrt{s_{\mathrm{NN}}} = 5.02$ TeV", *Phys. Lett. B* **772** (2017) 567–577, arXiv:1612.08966 [nucl-ex].